Microstructural investigation of Sr-modified Al-15wt%Si alloys in the range from micrometer to atomic scale

M. Timpel[a,*], N. Wanderka[a], G.S. Vinod Kumar[a,b], J. Banhart[a,b],

[a] *Helmholtz-Zentrum Berlin für Materialien und Energie GmbH, Hahn-Meitner-Platz 1, 14109 Berlin, Germany*
[b] *Technische Universität Berlin, Werkstoffwissenschaften und -Technologien, Hardenbergstr. 36, 10623 Berlin, Germany*

Abstract

Strontium-modified Al-15wt%Si casting alloys were investigated after 5 and 60 minutes of melt holding. The eutectic microstructures were studied using complementary methods at different length scales: focused ion beam-energy selective backscattered tomography, transmission electron microscopy and three-dimensional atom probe. Whereas the samples after 5 minutes of melt holding show that the structure of eutectic Si changes into a fine fibrous morphology, the increase of prolonged melt holding (60 minutes) leads to the loss of Sr within the alloy with an evolution of an unmodified eutectic microstructure displaying coarse interconnected Si plates. Strontium were found at the Al/Si eutectic interfaces on the side of the eutectic Al region, measured by three-dimensional atom probe. The new results obtained using three-dimensional atom probe shed light on the location of Sr within the Al-Si eutectic microstructure.

Keywords:

*Corresponding author
Email address: melanie.timpel@helmholtz-berlin.de (M. Timpel)

1. Introduction

Al-Si alloys are widely used for commercial applications mainly due to their low density and good mechanical and processing properties. Modification of Al-Si alloys by addition of Na or Sr is being applied industrially to further improve the mechanical properties of these materials [1]. It is known that minor additions of modifying elements transform the eutectic Si from a coarse plate-like network into a finer, more fibrous morphology [2, 3]. In addition to modification of the eutectic Si, the microstructure is also critically influenced by the casting parameters [4] and by additional alloying elements [5, 6].

Although the discovery of the modification effect dates back to 1921 [7] the exact mechanism of eutectic modification is not completely understood. Many possible mechanism of this technologically important transformation have been published [3, 8–13]. One of the most widely accepted models is the impurity-induced twinning theory according to which the impurity atoms are adsorbed at the growth steps of Si crystals growing by the twin plane re-entrant edge (TPRE) mechanism [3, 14]. The high twin density in Si fibers would require Sr atoms to be distributed rather uniformly within the Si phase. Besides the effect of Sr addition on the growth of eutectic Si, recent studies have confirmed that Sr also changes significantly the nucleation behavior of the eutectic phases [15]. It is proposed that the addition of Sr deactivates AlP [12] and/or oxide bifilms [13] as favoured nucleation sites for eutectic Si. Thus, Si is forced to nucleate at a lower temperature on some unknown

substrate and grow as a fine, fibrous eutectic Si with high twin density [16]. In order to confirm one of the proposed mechanisms, there is great interest in analysing the local distribution of the modifying element within the Al-Si eutectic and at the Al/Si eutectic interfaces. However, at the concentrations used for eutectic modification (80-120 ppm Sr in hypoeutectic Al-Si alloys [1]) analytic methods that provide compositional information on the nanoscale such as secondary ion mass spectrometry (SIMS) and analytical transmission electron microscopy (TEM) are not sensitive enough. Phase analysis by selective dissolution of both eutectic phases and subsequent atomic absorption spectroscopy indicates that the modifier Sr segregates preferentially within the Si phase during solidification of the modified eutectic [17]. However, in that study no information on the local distribution of Sr within the Si phase could be given. Recently, elemental mapping using X-ray fluorescence microscopy (μ-XRF) was used with a spatial resolution below 100 nm to investigate the Sr distribution in an Al-10Si-1Cu (wt%) alloy modified by 250 ppm Sr [18]. It was reported that Sr segregates exclusively within the eutectic Si and the distribution of Sr within this phase is approximately homogeneous.

This study reports mainly on three-dimensional atom probe (3D-AP) tomography measurements of the elemental distributions in a Sr-modified Al-15wt%Si alloy after 5 and 60 min of melt holding. The Sr distribution in specimens containing Al/Si eutectic interfaces was investigated. In addition, the development of the Al-Si eutectic microstructure was characterized by focused ion beam-energy selective backscattered (FIB-EsB) tomography as a complementary method providing three-dimensional (3D) information from

a volume of about 10^3 μm^3.

2. Experimental

The preparation of Sr-modified Al-15wt%Si alloy castings is described in detail in Ref. 19. After addition of the modifier Sr, the melt was cast into cylindrical rods, the first part after 5 min of melt holding and the second part after 60 min of holding. The samples used for chemical analysis were taken from the solidified castings. The chemical composition (in wt%) of the as-cast alloy was determined by inductively coupled plasma-atomic emission spectroscopy (ICP-AES), and is given in Table 1. For atom probe analysis, the castings were sectioned perpendicular to the rod axes and cut into pieces of $0.2\times0.2\times10$ mm^3. These pieces were then mechanically polished using diamond lapping films with 6 μm and 1 μm particle diameter to achieve tip radii of less than 5 μm, see Fig. 1(a). By applying this pre-sharpening step, the need for removal of excess bulk material during FIB milling was reduced. In order to prepare thin needles suitable for 3D-AP analysis containing the required microstructural features such as Al/Si eutectic interfaces, the final specimen sharpening was performed using a Zeiss 1540EsB CrossBeam® workstation. FIB milling and in-situ monitoring by SEM imaging were done using a method similar to that described in Ref. 20. Defined sample rotation and SEM imaging were used to identify the location of Al/Si eutectic interfaces to be analysed by atom probe and to keep track of a specific interface during the FIB milling steps. Tip sharpening was stopped after an Al/Si eutectic interface appeared at the apex of the specimen with a final radius of curvature below 50 nm, see Fig. 1(b). 3D-AP analyses were

performed in vacuum of 10^{-8} Pa at 60 K temperature with a pulse fraction of 20 % and a pulse repetition rate of 1 kHz. A Tomographic Atom Probe (3D-AP) by CAMECA was employed [21]. Additional information about the eutectic microstructure of the alloys was obtained by FIB-EsB tomography as described in Ref. 19. The in-lens EsB detector for the detection of elastically backscattered (high-angle) electrons produces a composition-weighted, high-resolution signal at a length scale of a few tens of nanometers in the x-y imaging plane. The 3D evolution of the eutectic microstructure for both holding times was visualized with its entire constitution of binary Al-Si eutectic and intermetallic impurity phases. The structural and chemical analysis of microconstituents present in the alloy were carried out using a Philips CM30 transmission electron microscope operating at 300 kV which was equipped with an EDAX Genesis energy dispersive X-ray spectroscopy (EDX) system. The crystal structure of the constituent eutectic phases was determined by selected area electron diffraction (SAED) in the TEM.

3. Results and Discussion

In order to study the development of the eutectic microstructure for different times of melt holding, the alloys were first characterized by optical microscopy. Typical optical micrographs obtained from both microstructures after 5 min and 60 min of melt holding are shown in Fig. 2(a) and (b), respectively.

According to the modification rating system that classifies the eutectic Si structures commonly observed in commercial castings by a number from one to six [22], the microstructure shown in Fig. 2(a) corresponds to 'partially

modified' from lamellar Si plates into a fine fibrous Si morphology corresponding to rating number 4. A mixed structure of thin Si platelets and fibrous Si is clearly visible, indicating a gradual change of the Si structure from plates into fibers. The modified Si platelets appear to break down into smaller segments. This becomes clearly visible on the polished surface (marked by arrows in Fig. 2(a)). To achieve a well-modified structure in hypoeutectic alloys, the Sr level is generally in the range of about 80-120 ppm Sr [1]. Due to a low Sr level after 5 min (62 ppm Sr) and the high eutectic volume fraction in the investigated alloys, it is not unexpected that locally the modification effect could be lost and therefore the eutectic microstructure is not completely modified. It is evident from Fig. 2(b) that after 60 min of melt holding the eutectic Si is much coarser and exhibits a typical unmodified, plate-like morphology (modification rating number 2). The longer holding time leads to a reduction of the Sr level within the alloy to 1 ppm and thus to the formation of an unmodified eutectic microstructure displaying coarse eutectic Si. It is suspected that Sr is lost by oxidation during the prolonged melt holding after the addition of the modifier.

Figures 3(a) and (b) demonstrate in 3D the microstructure of both investigated alloys by means of FIB-EsB tomography. SEM imaging of two-dimensional FIB slices using the EsB detector provides compositional contrast and hence makes visible not only the eutectic Si but also intermetallic impurity phases with a resolution of 50 nm and less.

After 5 min of melt holding (see Fig. 3(a)), the eutectic Si forms an interconnected and highly branched fibrous network. Several thin Si platelets were also found within the volume of interest. The estimated volume fraction of eu-

tectic Si is about 12 vol% within the investigated volume of $21.2 \times 8.6 \times 15.9\ \mu m^3$.

According to Fig. 2(b), the 3D eutectic microstructure after 60 min of melt holding appears as unmodified eutectic microstructure displaying coarse interconnected Si plates (cyan in Fig. 3(b)). Intermetallic impurity phases, identified as Fe-rich α-phases using EDX and SAED in TEM (magenta in Fig. 3(b)), were found in conjunction with the eutectic Al-Si microstructure after 60 min of melt holding. One of the Fe-rich α-phases present in the unmodified eutectic microstructure is imaged using bright field TEM, see Fig. 4. The corresponding SAED pattern is displayed in the inset in Fig. 4. The structure was found to have a body-centered cubic unit cell, space group Im3 with a lattice parameter a=1.245 nm. The average chemical composition of the Fe-rich α-phase was analyzed by EDX in the TEM and corresponds to $Al_{12.1}(Fe, Mn)_{3.9}Si_2$.

This Fe-rich α-phase could not be observed within the fibrous network of modified eutectic Si after 5 min of melt holding. Previous investigations of the unmodified and Sr-modified microstructure revealed that the addition of Sr not only modifies the Si morphology but also changes significantly the size and distribution of Fe-rich intermetallics present in the eutectic microstructure [19, 23]. The estimated volume fractions of eutectic Si and Fe-rich α-phase in Fig. 3(b) are 12 vol% and 0.3 %, respectively.

Figure 5 shows a typical mass spectrum obtained from the 3D-AP analysis of the eutectic Al phase. Aluminum atoms were detected as $^{27}Al^+$ at 27 amu and $^{27}Al^{2+}$ at 13.5 amu. In addition, singly charged Al hydrides $(AlH)^+$ and $(AlH_2)^+$ appeared in the mass spectrum at 28 and 29 amu. A possible overlap with Si^+ can be ruled out since there is no significant peak at 30 amu from the

$^{30}Si^{+}$ isotope. For all experimental conditions described here, the Si atoms evaporated exclusively in the 2+ charge state, and no measurable quantity of Si hydrides was detected. The Si^{2+} isotopic ratios revealed abundances close to the natural ones. Therefore, there is no indication for an overlap between $^{28}Si^{2+}$ and $(AlH)^{2+}$, and between $^{29}Si^{2+}$ and $(AlH_2)^{2+}$, respectively. The local concentration of Si within the eutectic Al amounts to 1.64±0.03 at% Si, which is in the order of maximum solid solubility of Si in Al (1.59 at%) [24]. Beside the peaks stemming from Al and Si, an additional peak was always detected at 28.5 amu, which might originate from Fe evaporating as hydride $(FeH)^{2+}$. The peak identified as $(AlH)^{+}$ at 28 amu would superimpose on the Fe^{2+} and this will affect the estimate of the amount of Fe present in the eutectic Al phase. A quantitative analysis of the $^{28.5}(FeH)^{2+}$ peak only (after substraction of the background noise level) yields a local concentration of 0.09±0.01 at% Fe in Al. However, this value is not in accordance with the solute solubility of 0.01 at% Fe in Al at 600°C [24].

Figure 6 displays elemental maps of Si in the eutectic Al phase measured from the alloy after 5 min of melt holding in an analysed volume of 10×10×41 nm^3. The Al atoms were omitted for clarity. A three-dimensional reconstruction of a truncated Si-rich particle is shown using a cluster-search module developed by the FIM group in Rouen [25]. No Sr atoms were detected within this volume. The Si-rich particle shown in Fig. 6 contains 81.8±4.0 at% Si, as estimated from a very small volume (number of detected atoms $\sim$ 88). Since Al is insoluble in Si [24] and due to local magnification effects at the precipitate/matrix interface [26, 27] some Al atoms included in the cluster analysis should originate from the surrounding Al. Since the

volume of the truncated Si-rich particle is very small it is difficult to decide whether this Si-rich particle belongs either to eutectic Si or to the primary Si phase or shows the formation of a small Si-rich cluster in the eutectic Al solid solution. It can be taken for granted that no Sr is located at the Al/Si interface around this Si particle.

Another 3D-AP measurement of the alloy after 5 min of melt holding is given in Fig. 7. Elemental maps of Al, Si and Sr are displayed in an investigated volume of $14\times14\times45$ nm^3, which contains an interface. Enrichment of Sr at the interface is visible. In this analysis, a few Al atoms were also observed to evaporate in the 3+ charge state. Due to the different local environment and therefore different local electric field strengths at the tip surface, this could affect the appearance of charge states and formation of hydrides. Strontium atoms were found to evaporate as doubly charged isotopes mainly observed between 43 and 44 amu. Along this interface, additional peaks stemming from oxygen and oxygen compounds were detected such as $^{16}O^+$, $^{17}OH^+$, $^{21.5}AlO^{2+}$, $^{23.5}SiOH_3{}^{2+}$ and $^{43}AlO^+$ in small amounts. The total concentration of oxygen is about 2 at% but the O atoms are not shown in Fig. 7. Furthermore, singly charged Ga ($^{69}Ga^+$, $^{71}Ga^+$) isotopes were detected, most likely an artefact caused by Ga implantation during FIB-based specimen preparation.

A typical 3D-AP analysis obtained from the alloy after 60 min of melt holding is shown in Fig. 8. The reconstruction of Al, Si and Sr atom positions within a volume of $14\times14\times20$ nm^3 (see Fig. 8(a)) indicates an Al/Si eutectic interface.

FIB-EsB tomography of the alloy after 60 min of melt holding clearly

reveals an unmodified structure of eutectic Si, see Fig. 3(b). This is expected since the chemical analysis shows a considerable loss of Sr after 60 min of melt holding (1 ppm Sr, see Table 1). However, the 3D-AP analysis of the Al-Si eutectic clearly indicates that Sr is enriched at the Al/Si eutectic interface.

Since the specimens investigated in the present 3D-AP study were prepared by site-specific FIB milling, we expect both eutectic Al and eutectic Si to be field-evaporated during the 3D-AP analyses. However, the contents of Si within the investigated volumes appear too low. In a previous study, it has been found that undefined field evaporation occurs for high-resistivity Si specimens whenever short voltage pulses as usually used in the conventional atom probe are applied [28]. Since a shortage of Si was measured in the present study, it is assumed that field evaporation of eutectic Si takes place in bursts contributing to multiple events that cannot be detected due to the limitation of the detector. Therefore, it was not possible to obtain quantitative microchemical information about the eutectic Si phase and its location in the investigated volumes. Despite these problems with defined field evaporation of the eutectic Si, the Sr segregation at the Al/Si eutectic interface is evident (see Figs. 7 and 8). Based on several measurements it can be concluded that accurate atom detection starts only after the eutectic Si has been field-evaporated completely. Strontium atoms were always found at the Al/Si interface on the side of the eutectic Al region. Although we are not able to observe the Sr distribution on the side of the eutectic Si region, a smooth transition of Sr concentration into the eutectic Si is assumed. However, by comparison of our results with the results reported in Ref. 18 we can neither confirm nor exclude a nearly homogenous distribution of Sr

throughout the modified Si fibers. Assuming that Sr is homogenously distributed within the eutectic Si (∼12 vol%), we can estimate that after 5 min of melt holding this would imply a local amount of about 0.02 at% Sr within the eutectic Si phase. The results of 3D-AP analyses clearly show Sr located at the interfaces. Therefore, we do not expect a considerable amount of Sr inside the eutectic Si.

Further work is required to clarify the inter- and intra-phase concentrations of Sr within the eutectic microstructure. Especially laser-assisted atom probe analysis has to be carried out in order to confirm the results obtained by voltage-pulsed atom probe analysis.

4. Summary

The alloy Al-15wt%Si with addition of Sr as modifier has been investigated after 5 and 60 min of melt holding. Three-dimensional microscopy techniques ranging from the sub-100 nm scale (FIB-EsB tomography) to the atomic scale (3D-AP) were applied to investigate the eutectic microstructure. Whereas FIB-EsB tomography illustrates the transformation of the eutectic Si morphology under the influence of Sr, the location of Sr is investigated by 3D-AP. The fibrous eutectic modification obtained after 5 min is lost after 60 min due to Sr oxidation during prolonged melt holding. An enrichment of Sr was still found at the Al/Si interface on the side of the eutectic Al region, not only in the alloy held for 5 min but also after 60 min of melt holding. The modified Al-Si eutectic microstructure of the alloy held for 5 min exclusively exhibits binary Al-Si eutectic in contrast to the sample after 60 min of melt holding where the Fe-rich α-phase was found located within the Al-Si

eutectic. In addition, quantitative analyses of eutectic Si and Fe-rich α-phase were carried out.

References

[1] G. K. Sigworth, The Modification of Al-Si Casting Alloys: Important Practical and Theoretical Aspects, Int J Metalcast 2 (2008) 19–41.

[2] L. F. Mondolfo, Nucleation in Eutectic Alloys, J Aust Inst Met 10 (1965) 169–177.

[3] S. Z. Lu, A. Hellawell, The Mechanism of Silicon Modification in Aluminum-Silicon Alloys: Impurity Induced Twinning, Metall Mater Trans A 18 (1987) 1721–1733.

[4] S. G. Shabestari, M. Keshavarz, M. M. Hejazi, Effect of strontium on the kinetics of formation and segregation of intermetallic compounds in A380 aluminum alloy, J Alloy Compd 477 (2009) 892–899.

[5] M. H. Mulazimoglu, N. Tenekedjiev, B. Closset, J. E. Gruzleski, Studies on the Minor Reactions and Phases in Strontium-treated Aluminium-Silicon Casting Alloys, Cast Metals 6 (1993) 16–28.

[6] W. Khalifa, F. H. Samuel, J. E. Gruzleski, Iron intermetallic phases in the Al corner of the Al-Si-Fe system, Metall Mater Trans A 34 (2003) 807–825.

[7] A. Pacz, U.S. Patent No.1387900 (1921).

[8] R. E. Search, New Aluminum-Silicon Alloys, Met Ind 20 (1922) 183–185.

[9] E. Schulz, Mikroskopische Untersuchungen bei der Veredelung von Silumin, Z Metallkde 39 (1949) 123–125.

[10] B. M. Thall, B. Chalmers, Modification in Aluminium Silicon Alloys, J Inst Metals 77 (1950) 79–97.

[11] V. d. L. Davies, J. West, Influence of Small Additions of Sodium on the Surface Tension of Aluminium and Aluminium-Silicon Alloys, J Inst Metals 92 (1963-64) 208–210.

[12] Y. H. Cho, H. C. Lee, K. H. Oh, A. K. Dahle, Effect of Strontium and Phosphorus on Eutectic Al-Si Nucleation and Formation of β-Al_5FeSi in Hypoeutectic Al-Si foundry alloys, Metall Mater Trans A 39A (2008) 2435–2448.

[13] J. Campbell, Discussion of "The Modification of Al-Si Casting Alloys: Important Practical and Theoretical Aspects", AFS Int J Metalcast 3 (2009) 65–77.

[14] L. M. Hogan, H. Song, Aluminum Grain Structures in Al-Si Eutectic Alloys, Acta Metall 35 (1987) 677–680.

[15] A. K. Dahle, K. Nogita, J. W. Zindel, S. D. McDonald, L. M. Hogan, Eutectic Nucleation and Growth in Hypoeutectic Al-Si Alloys at Different Strontium Levels, Metall Mater Trans A 32 (2001) 949–960.

[16] J. Campbell, Discussion of "Effect of Strontium and Phosphorus on Eutectic Al-Si Nucleation and Formation of β-Al_5FeSi in Hypoeutectic Al-Si Foundry Alloys", Metall Mater Trans A 40 (2009) 1009–1010.

[17] L. Clapham, R. W. Smith, Segregation Behavior of Strontium in Modified and Unmodified Al-Si Alloys, J Cryst Growth 92 (1988) 263–270.

[18] K. Nogita, H. Yasuda, K. Yoshida, K. Uesugi, A. Takeuchi, Y. Suzuki, A. K. Dahle, Determination of strontium segregation in modified hypoeutectic Al-Si alloy by micro X-ray fluorescence analysis, Scripta Mater 55 (2006) 787–790.

[19] M. Timpel, N. Wanderka, B. S. Murty, J. Banhart, Three-dimensional visualization of the microstructure development of Sr-modified Al-15Si casting alloy using FIB-EsB tomography, Acta Mater 58 (2010) 6600–6608.

[20] F. Pèrez-Willard, D. Wolde-Giorgis, T. Al-Kassab, G. A. Lopez, E. J. Mittemeijer, R. Kirchheim, D. Gerthsen, Focused ion beam preparation of atom probe specimens containing a single crystallographically well-defined grain boundary, Micron 39 (2008) 45–52.

[21] D. Blavette, B. Deconihout, A. Bostel, J. M. Sarrau, M. Bouet, A. Menand, The tomographic atom probe - A quantitative 3-dimensional nanoanalytical instrument on an atomic scale, Rev Sci Instrum 64 (1993) 2911–2919.

[22] G. K. Sigworth, Determining Grain Size and Eutectic Modification in Aluminium Alloy Castings, Mod Cast 77 (1987) 23–25.

[23] S. McDonald, Eutectic Solidification and Porosity Formation in Unmodified and Modified Hypoeutectic Aluminium-Silicon Alloys, Ph.D. thesis, 2002.

[24] M. Hansen, K. Anderko, Constitution of Binary Alloys, 1985.

[25] X. Sauvage, G. Dacosta, R. Z. Valiev, 3d atom probe investigation of cementite dissolution in a pearlitic steel processed by high pressure torsion, in: Y. T. Zhu, T. G. Langdon, R. Z. Valiev, S. L. Semiatin, D. H. Shin, T. C. Lowe (Eds.), 3rd International Symposium on Ultrafine Grained Materials, TMS 2004 Annual Meeting, Warrendale, Pennsylvania, USA, 2004, pp. 31–36.

[26] M. K. Miller, M. G. Hetherington, Local Magnification Effects in the Atom Probe, Surf Sci 246 (1991) 442–449.

[27] F. De Geuser, W. Lefebvre, F. Danoix, F. Vurpillot, B. Forbord, D. Blavette, An improved reconstruction procedure for the correction of local magnification effects in three-dimensional atom-probe, Surf Interface Anal 39 (2007) 268–272.

[28] A. J. Melmed, M. Martinka, S. M. Girvin, T. Sakurai, Y. Kuk, Analysis of high resistivity semiconductor specimens in an energy-compensated time-of-flight atom probe, Appl Phys Lett 39 (1981) 416–417.

Table Captions

Table 1: Fe concentration (in wt%) and additional impurity levels (in ppm) of the Sr-modified Al-15Si alloys investigated.

Tables

Table 1: **Fe concentration (in wt%) and additional impurity levels (in ppm) of the Sr-modified Al-15Si alloys investigated.**

Alloy	Fe	Al-Si	Cu	Mn	Mg	Zn	Ga	Pb	Sr
	wt%		ppm						
Sr, 5 min	0.165	Balance	73	116	11	159	167	75	62
Sr, 60 min	0.165	Balance	74	118	<1	161	167	79	1

Figures

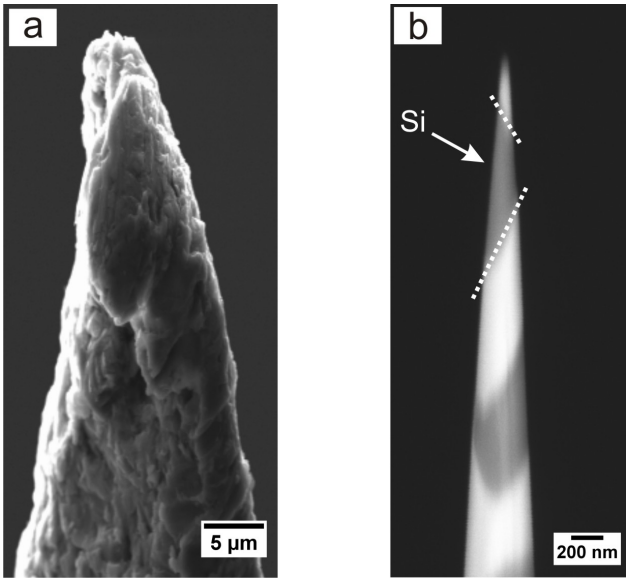

Figure 1: SEM images of atom probe specimen preparation steps: (a) Mechanically pre-sharpened specimen and (b) specimen after final FIB sharpening. The apex of the tip contains Al/Si eutectic interfaces (indicated by dotted lines).

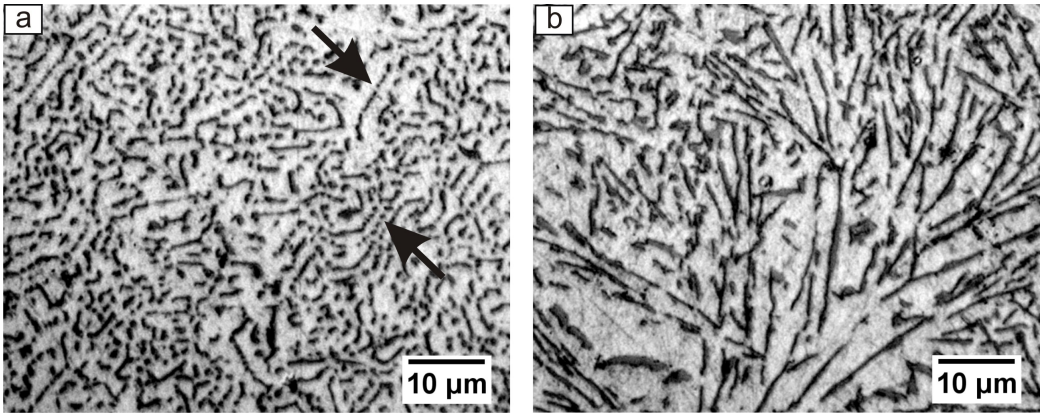

Figure 2: Optical micrographs of the Al-15Si eutectic microstructure (grey=Al, black=Si): (a) Fine fibrous Si morphology obtained after 5 min of melt holding. (b) Coarse lamellar Si structure obtained after 60 min of melt holding. The arrows in (a) indicate the gradual change from Si plates into aligned rows of individual fibers.

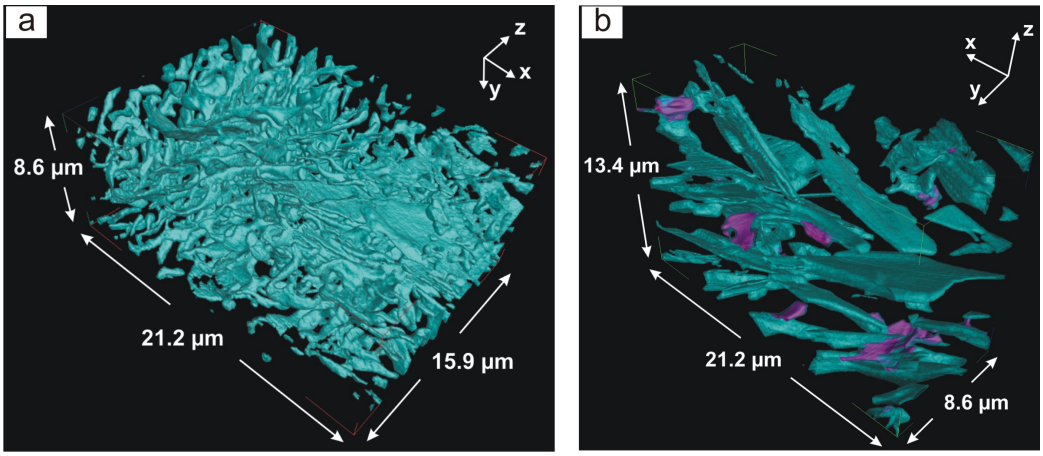

Figure 3: Three-dimensional visualization of the Al-15Si eutectic microstructure obtained by FIB-EsB tomography: (a) Fibrous network of eutectic Si obtained after 5 min of melt holding. (b) Coarse interconnected Si plates (in cyan) and Fe-rich α-phases (in magenta) obtained after 60 min of melt holding.

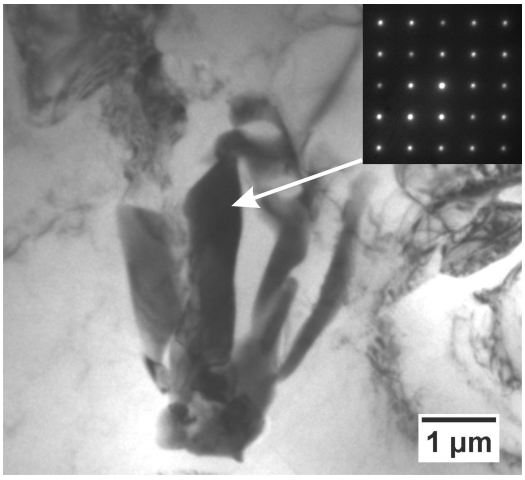

Figure 4: Bright field TEM image of Fe-rich α-phase embedded in eutectic Al obtained after 60 min of melt holding. The [100] zone axis SAED pattern of the Fe-rich α-phase is shown in the inset.

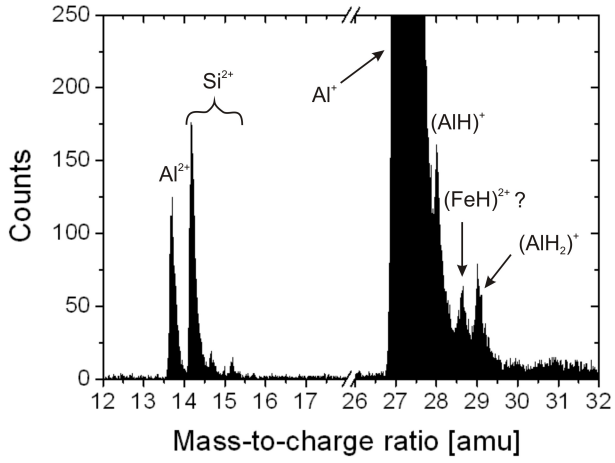

Figure 5: Typical mass spectrum obtained from the eutectic Al phase of the investigated Al-15Si alloy after 5 and 60 min of melt holding.

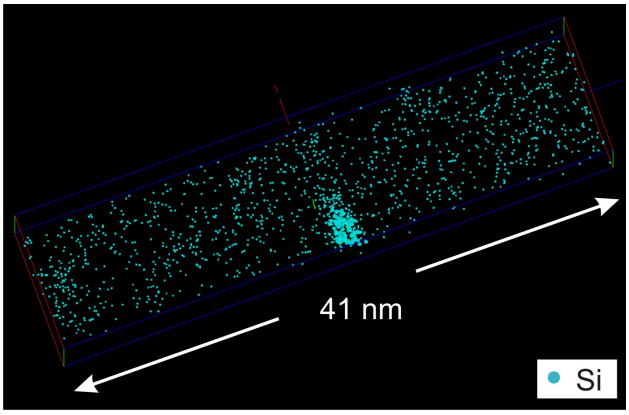

Figure 6: Three-dimensional reconstruction of Si atom positions and a Si-rich cluster within the eutectic Al in an analysed volume of $10\times10\times41$ nm^3 obtained after 5 min of melt holding. Threshold for Si clusters was >21 at%. The Al atoms were omitted for clarity.

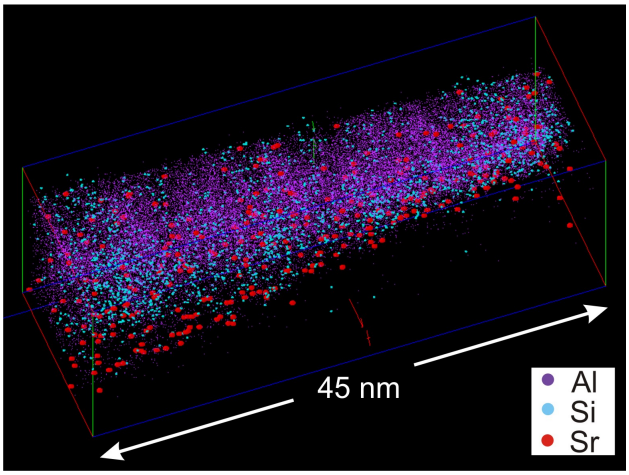

Figure 7: Three-dimensional elemental maps of Al, Si and Sr in a volume of $14\times14\times45$ nm^3 obtained after 5 min of melt holding. Strontium enrichment at the interface is visible.

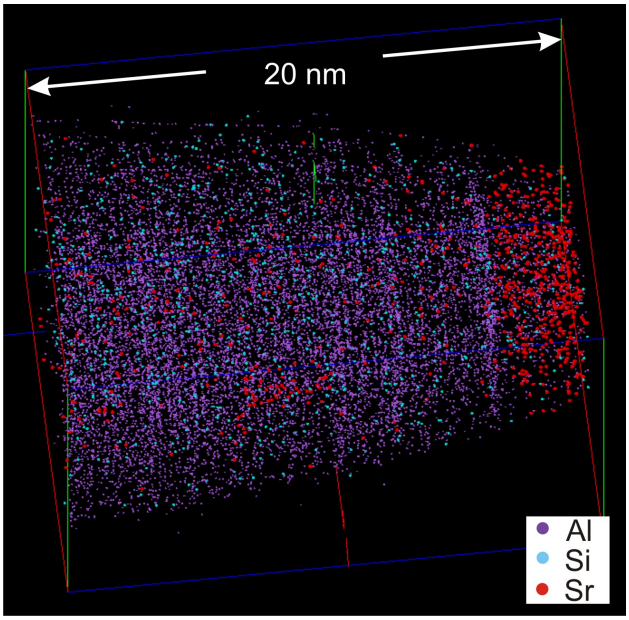

Figure 8: Three-dimensional elemental maps of Al, Si and Sr in a volume of $14 \times 14 \times 20$ nm^3 obtained after 60 min of melt holding.